Progress In Electromagnetics Research C, Vol. 173, 266–278, 2026
PIER C

(Received 29 June 2026, Accepted 21 August 2026, Scheduled 17 September 2026)

Design and Experimental Characterization of a Compact Quad-Port UWB-MIMO Antenna with Dual-Band Notches

Sunitha Mandava[1,*], Thotakura Sushma[2], Rajesh Gogineni[3], Chunduri Kirankumar[4], Ramesh Babu Sadineni[1], and Veeravalli Ramakoteswara Rao[5]

[1]*Department of Electronics & Communication Engineering, RVR & JC College of Engineering, Guntur 522019, India*
[2]*Department of Electronics & Communication Engineering, PVP Siddartha Institute of Technology, Vijayawada, India*
[3]*Department of Electronics & Communication Engineering, Dhanekula Institute of Engineering and Technology, Ganguru, India*
[4]*Department of MCA, Koneru Lakshmaiah Education Foundation, Vaddeswaram, India*
[5]*Department of Mechanical Engineering, RVR & JC College of Engineering, Guntur 522019, India*

ABSTRACT: This paper presents a compact $39 \times 39\,\text{mm}^2$, quad-port, ultra-wideband (UWB) MIMO antenna with dual band-notches and enhanced inter-element isolation. Four orthogonally arranged microstrip-fed circular radiators are employed to reduce mutual coupling, while two U-shaped slots etched on each radiator suppress interference from the C-band (3.1–4.3 GHz) and Wireless LAN (5.2–5.6 GHz) bands. We investigate the antenna using Characteristic Mode Analysis via modal significance and modal current distributions. The proposed diversity antenna is evaluated using envelope correlation coefficient, diversity gain, total active reflection coefficient, channel capacity loss, multiplexing efficiency, and simulated group delay. The antenna achieves an impedance spectrum covering 2.9–10.6 GHz, radiation efficiency of 90%, gain of 5.2 dBi, ECC < 0.02, and isolation of -20 dB. The results demonstrate that the proposed antenna provides an effective combination of small size and high isolation, making it viable for UWB applications.

1. INTRODUCTION

Ultra-Wideband (UWB) technology has become an important candidate for high-speed wireless communication because of its wide operating bandwidth and capability to support high-data-rate transmission. The broad frequency spectrum offered by UWB systems has enabled their application in several areas, including wireless personal area networks, radar, indoor positioning, medical imaging, and other short-range wireless systems [1–5]. For such applications, the antenna is required to provide stable impedance characteristics over a wide frequency range while maintaining a compact physical structure.

However, the wide frequency coverage of UWB systems creates a potential problem because portions of the UWB spectrum overlap with existing wireless services. Interference from these coexisting systems can degrade the performance of the communication link. One effective approach for mitigating this problem is to incorporate frequency-rejection characteristics directly into the UWB antenna. In contrast to external filtering circuits, integrated band-notched structures can provide frequency-selective suppression without additional components. A band-notched UWB printed monopole antenna was reported using an integrated resonant structure to reject an undesired frequency range [6]. This approach demonstrated the feasibility of obtaining a stopband within a wideband antenna while retaining the required broadband response.

Subsequent studies investigated different geometrical techniques for generating one or more rejection bands. Planar UWB antennas with multiple notched bands have been developed by incorporating suitable resonant elements into the antenna geometry [7]. Dual band-notched characteristics have also been obtained in planar UWB monopole configurations, demonstrating that multiple interference regions can be selectively suppressed within a single antenna [8]. A coplanar waveguide (CPW)-fed dual band-notched UWB antenna was further reported, showing that the feeding structure and resonant elements can be appropriately designed to control rejected frequency regions [9]. These investigations established that modifying the antenna geometry can provide an integrated alternative to conventional external band-stop filtering.

Different forms of resonant loading have been subsequently explored to obtain controllable notch characteristics. Multiple band-rejected elements integrated into the feed line have been used to generate selective rejection while maintaining UWB operation [10]. Compact monopole configurations with variable notch characteristics have also been investigated, in which the rejection frequency can be controlled through appropriate geometrical modifications [11]. Similarly, a compact rectangular slot antenna with a variable band-stop response demonstrated another method for introducing frequency-selective suppression into a UWB antenna [12]. The requirement for suppressing more than two interfering frequency regions has also encouraged the development of compact antennas with multiple notches. A triple band-notched UWB antenna, for example, demonstrated the possibility of simultaneously controlling several rejected frequency regions within a compact radiating structure [13].

* Corresponding author: Sunitha Mandava (msunitha@rvrjc.ac.in).

The fundamental UWB radiating element is also important in achieving wide impedance bandwidth. Printed circular-disc monopole antennas have been investigated for UWB systems and have demonstrated the suitability of simple planar radiators for broadband operation [14]. Other compact wideband antenna configurations, including tapered-slot-fed annular-slot structures, have also been proposed for UWB applications [15]. In addition, tapered-shape slot antennas have been investigated to obtain compact broadband characteristics while maintaining an appropriate radiation response [16]. These studies indicate that the selection and modification of the radiating element, feeding structure, and ground plane play important roles in obtaining desired UWB impedance characteristics [17–20].

Although single-element UWB antennas with band-notched characteristics can effectively suppress interfering frequency bands, the increasing demand for high-capacity and reliable wireless communication has encouraged integrating UWB antennas with multiple-input multiple-output (MIMO) technology. MIMO systems employ multiple antenna elements to exploit spatial diversity and improve communication capacity and reliability [21–23]. However, the physical separation between antenna elements becomes limited when a MIMO antenna occupies a small area. Consequently, strong mutual coupling can occur between adjacent elements, which may adversely affect port isolation and the overall diversity performance [24, 25].

Several techniques have therefore been investigated to reduce mutual coupling in compact MIMO configurations. Parasitic structures, electromagnetic bandgap (EBG) structures, metamaterial-based elements, and other decoupling mechanisms have been employed to improve isolation between closely spaced antenna elements [27–30]. In particular, compact dual band-notched UWB-MIMO configurations have demonstrated that wideband operation, frequency-selective rejection, and enhanced isolation can be achieved within a single-antenna system [28]. Characteristic-mode-based techniques have also been applied to compact UWB-MIMO antennas to investigate the influence of the ground structure and characteristic modes on antenna performance [30]. Ground-plane modification provides another attractive approach because it can alter the surface-current distribution and suppress coupling without substantially increasing overall antenna dimensions [31, 32].

Characteristic Mode Analysis (CMA) provides a useful framework for investigating the electromagnetic behavior of conducting antenna structures. The theory separates the total current on the conducting body into independent characteristic modes, allowing the resonant behavior and radiation contribution of individual modes to be examined [33–35]. CMA has been employed in the design of multimode UWB antennas to identify dominant modes responsible for broadband operation [36]. Compact, low-profile, UWB antennas have also been studied using CMA, where the modal behavior provides useful information for understanding the antenna's operating mechanism [37]. Furthermore, the theory of characteristic modes has been applied to printed planar UWB quasi-monopole antennas to analyze their modal characteristics and explain broadband radiation behavior [38].

More recently, hybrid decoupling techniques combining a neutralization line with a defected ground structure have been used to enhance isolation in dual-band-notched UWB-MIMO antennas [39]; standalone defected ground structures have been employed to realize highly isolated two- and four-port UWB-MIMO antennas with WLAN and X-band notches [40]; self-isolated orthogonally arranged quad-port UWB-MIMO configurations have been reported to suppress dual X-band interference without dedicated decoupling elements [41–43]. The novelty and contributions of the proposed work are explicitly demonstrated by explicitly comparing the proposed antenna with our previous publications and other related designs. The revised manuscript highlights specific differences in the antenna configuration, notch-band frequencies, dual-notch implementation, isolation performance, and overall MIMO characteristics.

This study introduces a miniaturized, high-isolation, dual-band suppressed UWB-MIMO antenna. The design incorporates a modified circular radiator, resonant slots embedded within the radiator structure, and an optimized ground plane. These features collectively enable wideband operation, controllable notch bands, and reduced mutual coupling. The CMA was performed to evaluate the antennas' performance and illustrate how the characteristic modes directly improve the angle performance and notch generation. The proposed antenna has a broad impedance spectrum, very high isolation, low envelope correlation coefficient, stable radiation patterns, and very effective suppression of interfering bands, while allowing a compact antenna shape suited for 21st-century wireless devices.

2. UNIT ANTENNA ELEMENT

Figure 1 illustrates the final optimized structure of the proposed dual band-suppressed UWB antenna. The antenna uses a circular copper patch lithographed on an FR-4 substrate. The compact antenna occupies an area of $19.5\,\text{mm} \times 19.5\,\text{mm}$. The optimized geometrical parameters are: $Ls = 19.5\,\text{mm}$, $Ws = 19.5\,\text{mm}$, $a = 7.5\,\text{mm}$, $b = 3.9\,\text{mm}$, $c = 9\,\text{mm}$, $d = 7\,\text{mm}$, $e = 5.5\,\text{mm}$, $f = 3.2\,\text{mm}$, $g = 0.5\,\text{mm}$, $g1 = 5\,\text{mm}$, $g2 = 0.8\,\text{mm}$, $g3 = 8.5\,\text{mm}$, $Wf = 2\,\text{mm}$, $R = 3.3\,\text{mm}$, $R1 = 2.42\,\text{mm}$, $R2 = 4\,\text{mm}$, $Lf = 7.47\,\text{mm}$, and $W = 39\,\text{mm}$.

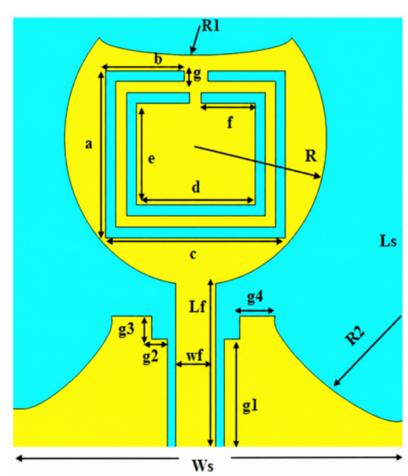

FIGURE 1. Suggested antenna geometry.

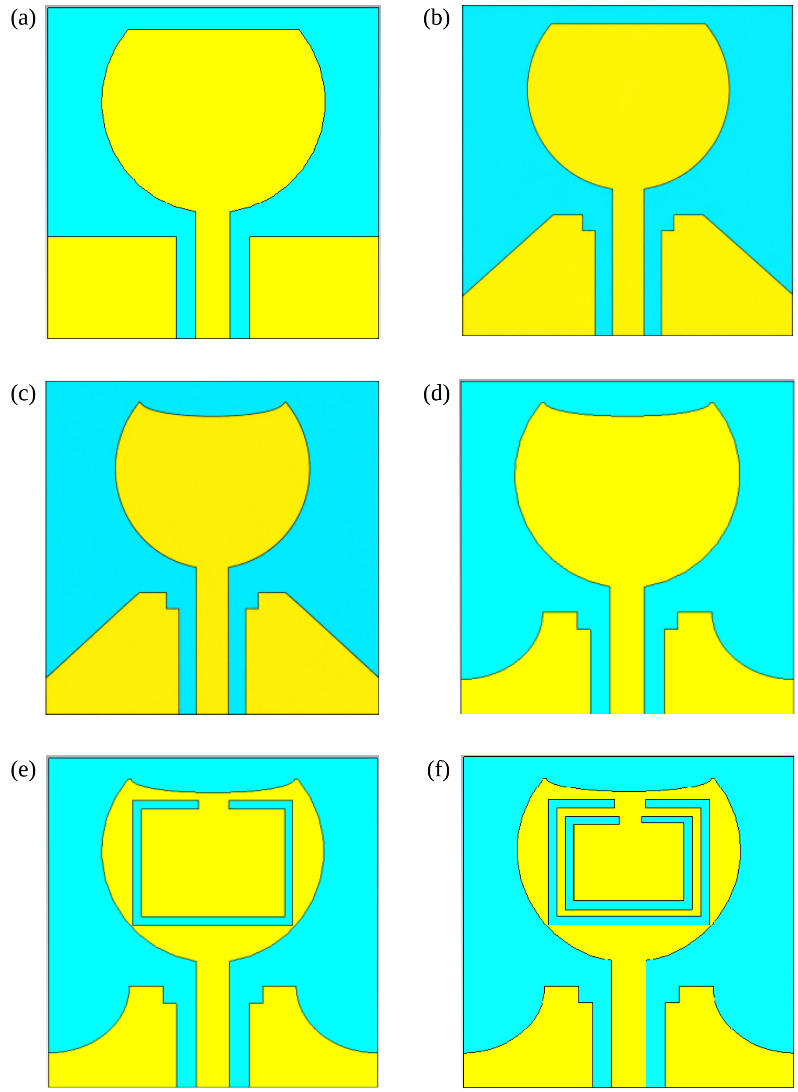

FIGURE 2. Unit antenna element evolution. (a) Ant-1, (b) Ant-2, (c) Ant-3, (d) Ant-4, (e) Ant-5, and (f) Ant-6.

TABLE 1. CST parametric-sweep table.

Parameter varied	Range	Expected effect
a	6.5–8.5 mm	3.1–4.3 GHz notch
c	8–10 mm	3.1–4.3 GHz notch
e	4.5–6.5 mm	5.2–5.6 GHz notch
d	6–8 mm	5.2–5.6 GHz notch

Table 1 validates the effective-current-path model, and a parametric study was performed by independently varying a, c, d, and e while keeping the remaining geometrical parameters unchanged. The first notch shifts toward lower frequencies with increasing a and c, whereas the second notch shifts toward lower frequencies with increasing d and e. This behavior agrees with Eqs. (1) and (2), since an increase in any of these dimensions increases the corresponding effective current path and consequently reduces the resonant frequency. The optimized values $a = 7.5\,\text{mm}$, $c = 9\,\text{mm}$, $d = 7\,\text{mm}$, and $e = 5.5\,\text{mm}$ provide notch frequencies centered approximately at 4.1 GHz and 5.5 GHz, respectively.

Figure 2 depicts the design evolution of the proposed antenna. Ant-1 had a circular radiator with a microstrip feed. To improve impedance matching, triangular ground-plane cuttings were introduced beside the feed line, resulting in Ant-2. Further enhancement is achieved in Ant-3 by incorporating a curved notch into the circular radiator, which increases the effective current path. By optimizing radiator and ground-plane modifications, Ant-4 was obtained, showing improved impedance matching and a wider bandwidth. To realize the band-notch functionality, Slot #1 is etched into Ant-4, forming Ant-5, which suppresses the 3.1–4.3 GHz downlink C-band. Subsequently, an additional open-ended U-slot (Slot #2) is introduced to obtain Ant-6, enabling dual-band rejection at 3.1–4.3 GHz and 5.2–5.6 GHz (WLAN). The approximate notch frequencies were initially estimated from the effective current-path model given by (1)–(4) and subsequently optimized through Computer Simulation Technology (CST) parametric simulations.

Derivation for the first U-slot (notch 1)

$$L_{\mathit{eff},1} = 2 \times (a) + c = 24\,\text{mm} \tag{1}$$

TABLE 2. Calculated R, L, C values.

	BW (GHz)	Resonance f_0 (GHz)	Q_0	R in Ω	L in nH	C in pF
First notch (3.1–4.3 GHz)	1.2	4.1	3.417	50	6.63	0.227
Second notch (5.2–5.6 GHz)	0.40	5.5	13.75	50	19.894	0.042

$$L_{eff,1} \approx \frac{\lambda_g}{2} \tag{1a}$$

$$\lambda_g = \frac{C_0}{f_{\text{notch1}}\sqrt{\varepsilon_{eff,1}}} \tag{1b}$$

$$f_{notch1} = c_0/2(2a+c)\sqrt{\varepsilon_{eff,1}}$$

Derivation for the inner U-slot (notch 2)

$$L_{eff,2} = 2 \times (d) + e \tag{2}$$

$$L_{eff,2} \approx \frac{\lambda_g}{2} \tag{3}$$

$$f_{notch2} = c_0/2(2a+c)\sqrt{\varepsilon_{eff,2}} \tag{4}$$

where (c_0) is the velocity of light in free space, and (*eff*) is the effective dielectric constant associated with the slot current path. The factor of two represents the approximately half-wavelength resonant condition of the open-ended slot.

Figure 3 depicts $|S_{11}|$ characteristics of Ant-1–Ant-6. Ant-1 provides an impedance bandwidth of approximately 5 GHz. After progressive structural optimization, Ant-2, Ant-3, and Ant-4 achieved UWB coverage from 2.9 to 10.6 GHz. The notch performance is realized in Ant-5 and Ant-6 by introducing two U-shaped slots, producing rejection bands at 3.1–4.3 GHz and 5.2–5.6 GHz, corresponding to the C-band and Wireless LAN, respectively.

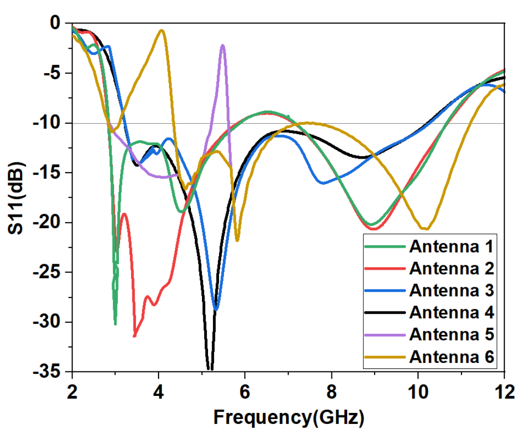

FIGURE 3. Simulated $|S_{11}|$.

2.1. Equivalent Circuit Analysis

An equivalent RLC circuit was constructed to describe the band-notching mechanism of the proposed dual band-suppressed UWB antenna, given in Figure 4(b). As demonstrated in Figure 4(a), the antenna without notch structures exhibited a real impedance closer to 50 Ω and a negligible imaginary component, ensuring effective impedance matching. After introducing notch elements, distinct series resonances were observed at 3.1–4.3 GHz and 5.2–5.6 GHz, where the imaginary impedance changed sign, resulting in band rejection (Figure 4(a)). The circuit was implemented in Advanced Design System (ADS), as depicted in Figure 4(c), and its response was compared with the CST simulation results.

The extracted RLC parameters and quality factor (Q_0) are calculated using Eqs. (4)–(6) and presented in Table 2.

$$f_{notch,i} = \frac{1}{2\pi\sqrt{L_i C_i}} \tag{5}$$

$$Q_0 = \frac{1}{2\pi f_{notch,i} R_i C_i} \tag{6}$$

$$\text{BW} = \frac{f_{notch,i}}{Q_0} \tag{7}$$

3. MIMO CONFIGURATION

A compact quad-port UWB-MIMO antenna was realized by arranging four antennas orthogonally to achieve polarization diversity, as shown in Figure 5. The proposed antenna covers the 2.9–10.6 GHz UWB range while introducing rejection bands at 3.1–4.3 GHz and 5.2–5.6 GHz. The orthogonal configuration provides excellent isolation, with S_{12} and S_{14} below -20 dB. Figure 5(b) shows the fabricated prototype. Simulated and measured outcomes, shown in Figure 6, are in close agreement.

The proposed antenna is a compact $39 \times 39\,\text{mm}^2$ quad-port UWB-MIMO configuration with four orthogonally arranged antenna elements. The central placement of the antenna elements maintains the required compact, symmetric MIMO configuration to achieve polarization diversity with high isolation. In a practical wireless device, remaining available printed circuit board (PCB) regions and multilayer PCB technology can be used for placing the radio frequency (RF) frontend and other electronic circuitry, while appropriate grounding and isolation can be maintained to minimize electromagnetic coupling. The proposed work primarily focuses on the antenna performance, and detailed system-level integration with electronic circuitry will be considered in future work.

4. RESULTS AND DISCUSSION

Figure 7 depicts surface currents at the notches. By exciting Port-1, strong current concentrations are observed around the outer slot at 3.1–4.3 GHz and the inner slot at 5.2–5.6 GHz. The

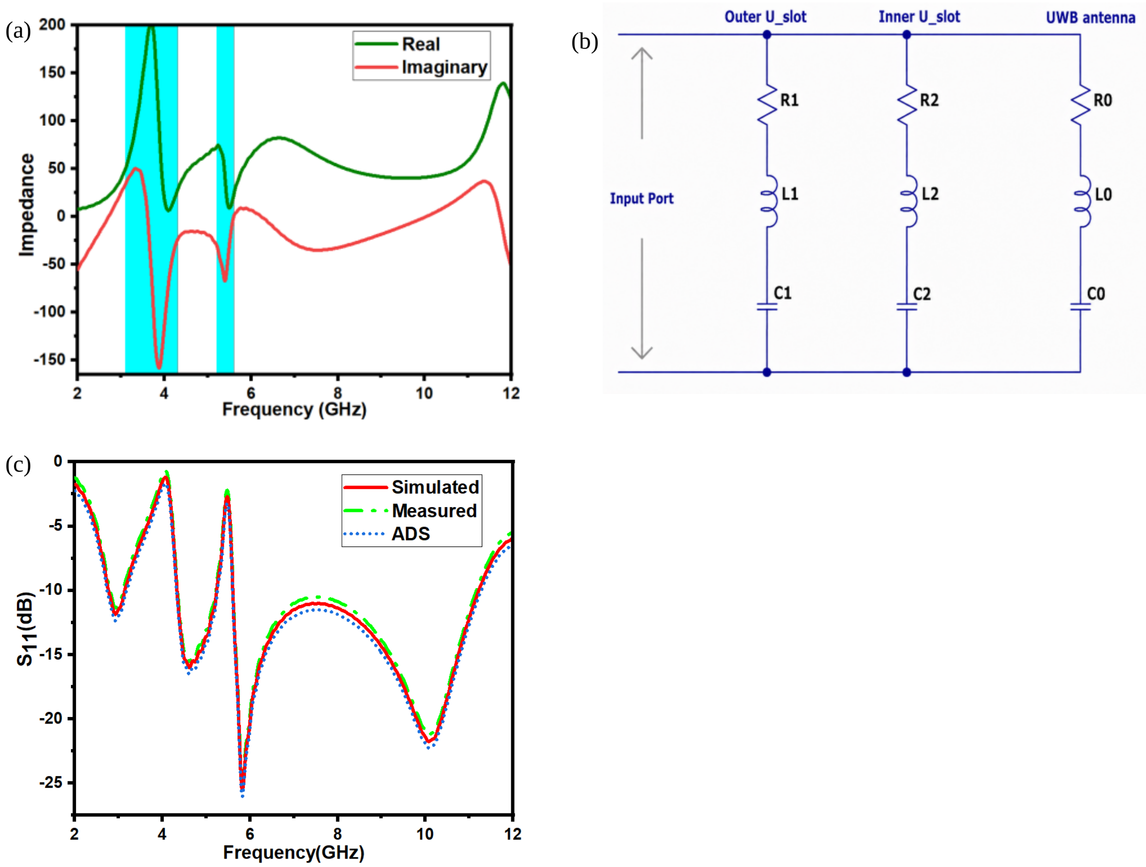

FIGURE 4. (a) Impedance curves without band notch elements, (b) equivalent circuit, and (c) comparison results of CST and ADS.

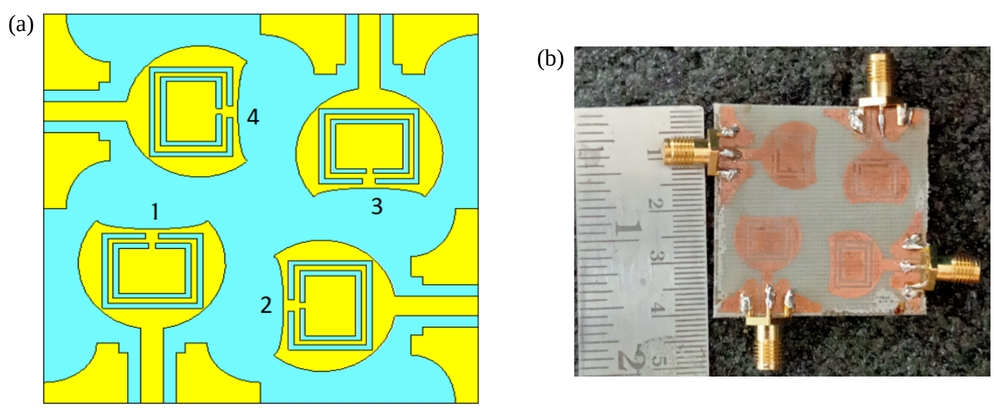

FIGURE 5. (a) Configuration of four-port UWB MIMO antenna and (b) prototype.

induced currents flow in opposite directions along slot boundaries, resulting in field cancellation and radiation suppression. Consequently, the antenna exhibits an effective band-rejection behavior at the corresponding notch frequencies.

Figure 8 depicts radiation characteristics of the suggested antenna at 3 GHz, 7 GHz, and 10 GHz of E- and H-planes. The co-polarization levels are notably higher than the cross-polarization levels, confirming satisfactory polarization performance.

Figure 9(a) depicts the peak gain response of the proposed antenna. Stable gain is achieved across the UWB band, except in 3.1–4.3 GHz and 5.2–5.6 GHz notched regions, where a pronounced decrease confirms effective band suppression. Simulated and measured gains are 4.5 dBi and 4 dBi, respectively, with minor deviations caused by fabrication and measurement imperfections. The antenna maintains approximately 90% radiation efficiency over the operating band, while the efficiency falls below 65% at the notched frequencies, validating the notch-band performance given in Figure 9(b).

4.1. Envelope Correlation Coefficient

Envelope correlation coefficient (ECC) is an important parameter for evaluating the diversity performance of a MIMO an-

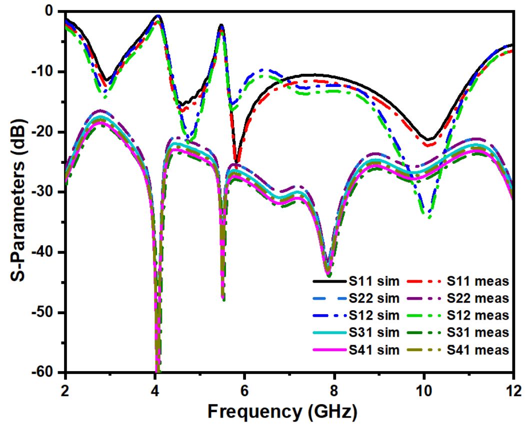

FIGURE 6. Simulated and measured S-parameters.

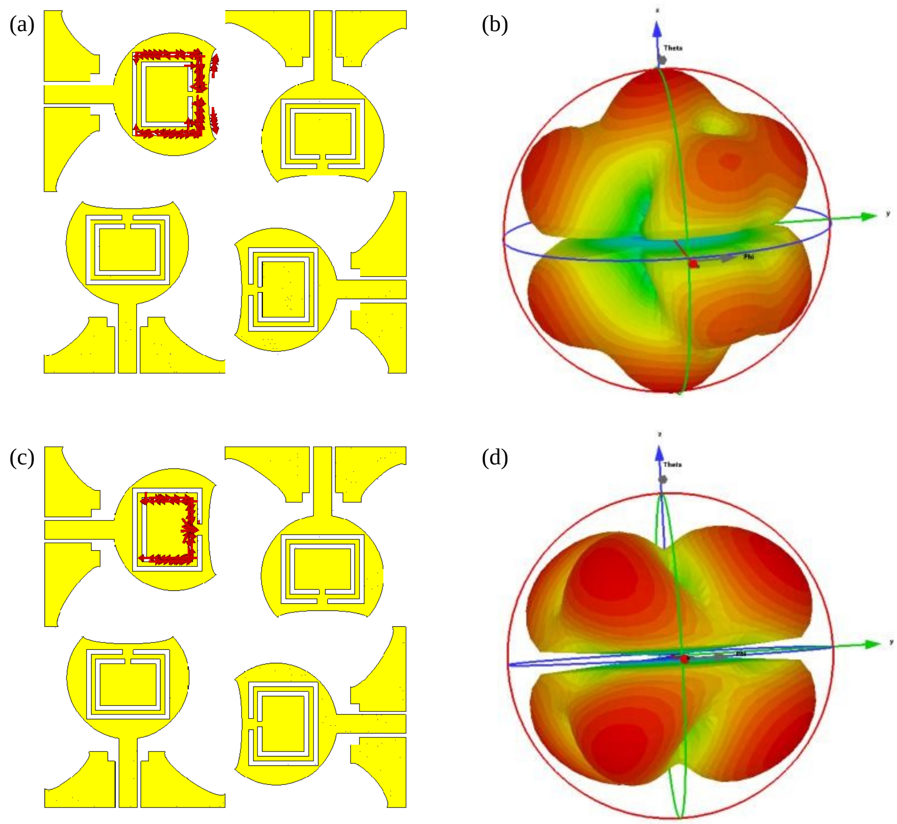

FIGURE 7. Simulated radiation patterns and surface-current distributions of the proposed antenna: (a) Surface-current distribution at 3.1–4.3 GHz, (b) surface-current distribution at 5.2–5.6 GHz, (c) 3-D radiation pattern at 3.1–4.3 GHz, and (d) 3-D radiation pattern at 5.2–5.6 GHz.

tenna. In this work, ECC is calculated from the simulated four-port S-parameter matrix rather than from far-field radiation data. Here, S_{ni} and S_{nj} represent complex S-parameters of the four-port antenna, and $*$ denotes the complex conjugate. The ECC was evaluated at each frequency for all six unique port pairs, namely 1-2, 1-3, 1-4, 2-3, 2-4, and 3-4. As shown in Figure 10(a), the ECC shows a pronounced peak of approximately 0.72 at around 2.45 GHz, corresponding to the 3-4 port pair, while the ECC values remain very low over most of the remaining frequency range. The maximum ECC occurs near the lower edge of the operating band, whereas the values within the principal UWB operating region are substantially lower. Although the peak value exceeds the commonly adopted ECC criterion of 0.5, it is confined to the lower-frequency region; therefore, the ECC performance should be reported separately for the complete frequency range and the intended UWB passband rather than stating a single value of ECC < 0.02 across the entire spectrum.

$$\mathrm{ECC}_{e,ij} = \frac{\left|\sum_{k=1}^{N} S_{ik}^{*} S_{jk}\right|^2}{\left(1-\sum_{k=1}^{N}|S_{ik}|^2\right)\left(1-\sum_{k=1}^{N}|S_{jk}|^2\right)} \tag{8}$$

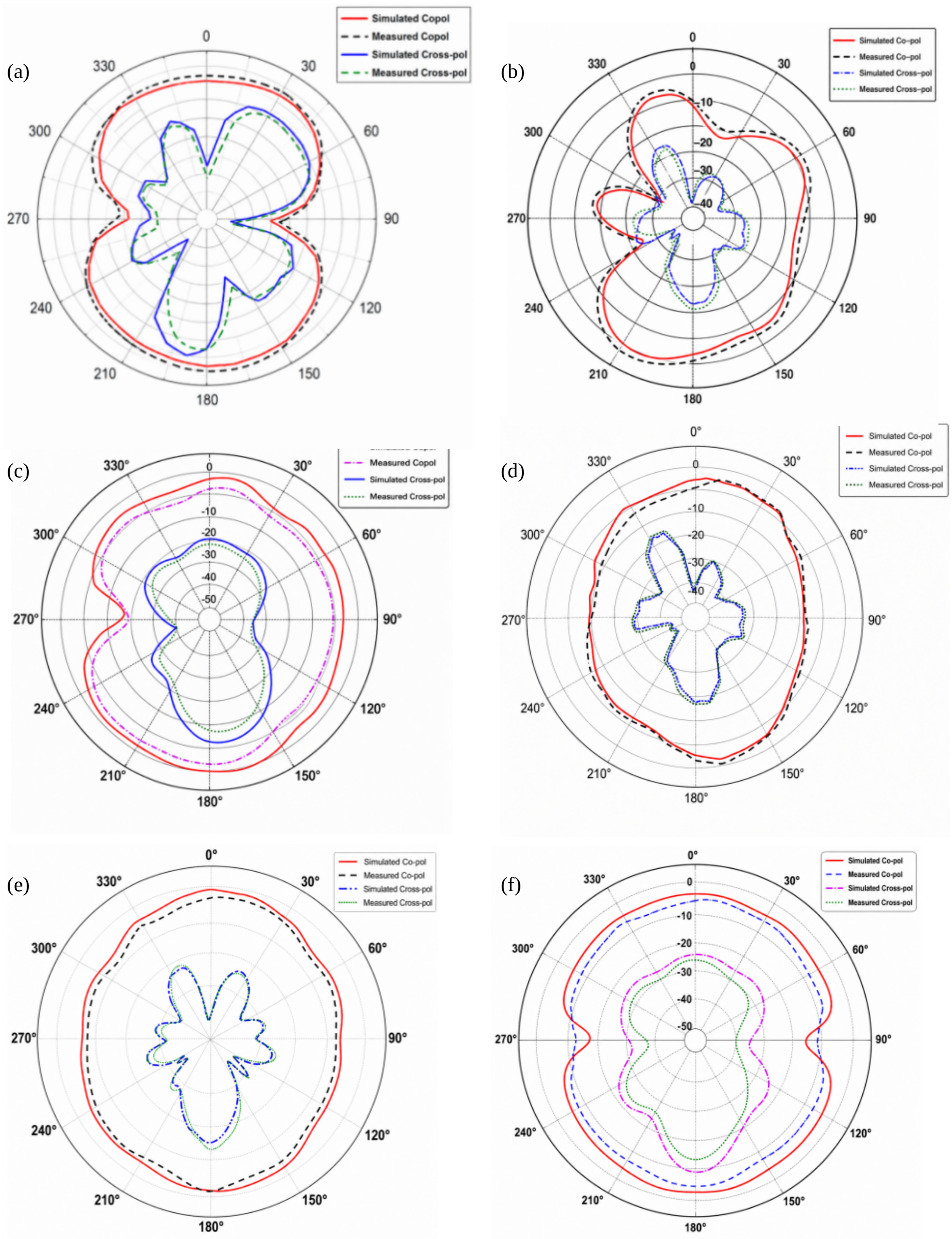

FIGURE 8. Radiation characteristics passband frequencies at (a) 3 GHz (E-plane), (b) 3 GHz (H-plane), (c) 7 GHz (E-plane), (d) 7 GHz (H-plane), (e) 10 GHz (E-plane), and (f) 10 GHz (H-plane).

4.2. Diversity Gain

Diversity gain quantifies the enhancement in the attained signal-to-noise ratio (SNR). ECC and diversity gain are interrelated, as shown in Eq. (8).

$$DG = 10\sqrt{1 - |\mathrm{ECC}_e|^2} \tag{9}$$

Figures 10(a) and (b) show that both ECCs are < 0.02, and DG is 9.98 dB across the entire frequency spectrum, except at notches. This demonstrates the efficacy of the reported UWB-MIMO antenna.

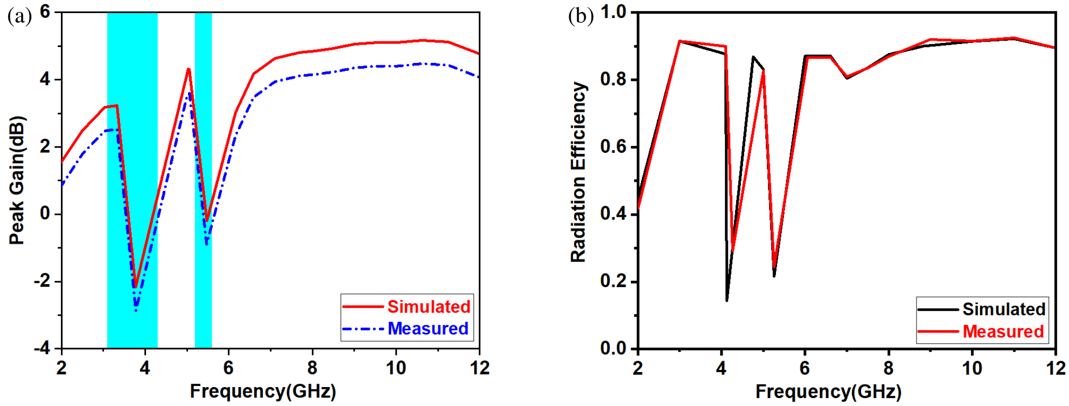

FIGURE 9. (a) Peak gain and (b) radiation efficiency.

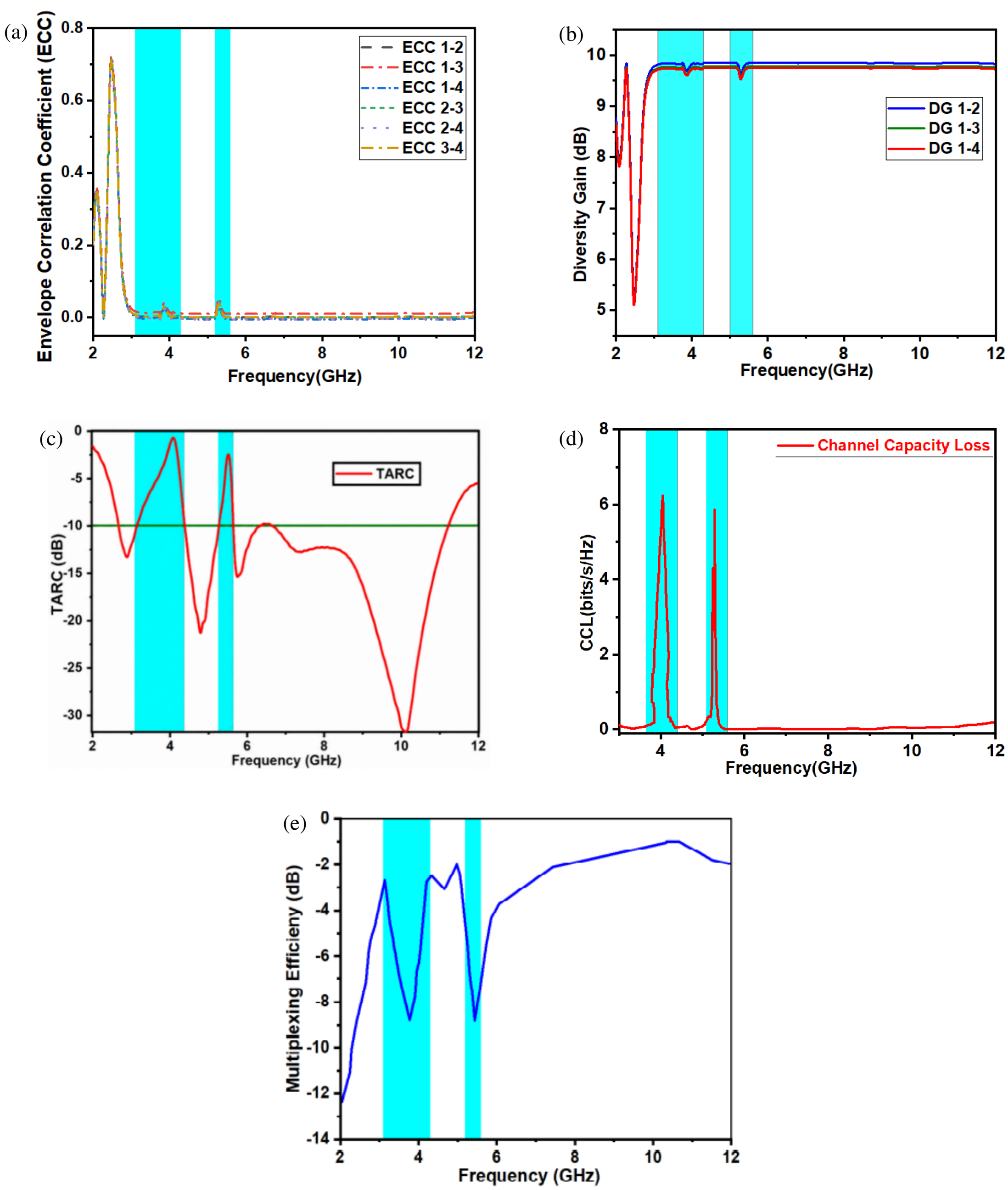

FIGURE 10. (a) ECC, (b) DG, (c) TARC, (d) CCL, and (e) multiplexing efficiency.

4.3. Total Active Reflection Coefficient (TARC)

Figure 10(c) shows that TARC evaluates the combined reflected power under simultaneous excitation of the four antenna ports. The complete four-port scattering matrix is represented by S, and for an excitation vector $a = [a_1, a_2, a_3, a_4]^T$. The TARC is calculated as

$$\text{TARC} = \sqrt{\frac{\sum_{i=1}^{4} \left| \sum_{j=1}^{4} S_{ij} a_j \right|^2}{\sum_{i=1}^{4} |a_i|^2}} \tag{10}$$

and expressed in dB as $20 \log_{10}(\text{TARC})$. The excitation amplitudes and relative phases are kept identical to those used in the corresponding full-wave simulation. The worst-case TARC is obtained from specified excitation cases over the useful UWB passband.

4.4. Channel Capacity Loss

Figure 10(d) depicts the CCL, which is evaluated from the complete four-port correlation matrix. The 4×4 matrix is constructed from the complex S-parameter data of the proposed antenna, and CCL is calculated using

$$\text{CCL} = -\log_2 \det \left(I - S^H S \right)$$

The calculation is performed at every frequency over the useful UWB passband. The maximum CCL and its corresponding frequency are reported to represent the worst-case channel-capacity performance.

4.5. Multiplexing Efficiency

Multiplexing efficiency is evaluated pairwise for all six unique port combinations of the quad-port MIMO antenna. For each pair, the two-port expression in the given equation is applied to the corresponding S-parameter subset. The minimum multiplexing efficiency among all six port pairs is reported as the worst-case value. Thus, the presented multiplexing-efficiency result represents the worst-performing port pair rather than an unlabeled single-port-pair response. Multiplexing efficiency for a two-port pair can be written as:

$$\eta_{\text{mux},ij} = \sqrt{(1 - |S_{ii}|^2 - |S_{ji}|^2)\,(1 - |S_{jj}|^2 - |S_{ij}|^2)}$$

where $i, j \in \{1, 2, 3, 4\}$ denote selected antenna ports.

For the six unique port pairs, Eq. (11) is evaluated as:

$$(1, 2),\ (1, 3),\ (1, 4),\ (2, 3),\ (2, 4),\ (3, 4).$$

For example, for ports 1 and 2:

$$\eta_{\text{mux},12} = \sqrt{(1 - |S_{11}|^2 - |S_{21}|^2)\,(1 - |S_{22}|^2 - |S_{12}|^2)}.$$

For ports 1 and 3:

$$\eta_{\text{mux},13} = \sqrt{(1 - |S_{11}|^2 - |S_{31}|^2)\,(1 - |S_{33}|^2 - |S_{13}|^2)}.$$

Two-port formulation is applied to each selected port pair of the four-port antenna. Then, define the reported worst-case value as

$$\eta_{\text{mux, worst}} = \min_{i<j} \left[\eta_{\text{mux},ij} \right] \tag{11}$$

over the six port pairs and specified operating frequencies.

The multiplexing efficiency in dB is calculated as

$$\eta_{\text{mux, dB}} = 10 \log_{10}(\eta_{\text{mux}})$$

Figure 10(e) shows that the multiplexing efficiency has dual-band notch features. Throughout the entire impedance bandwidth (2.9–10.6 GHz), excluding the notch frequencies, the multiplexing efficiency exceeds -3 dB, indicating that the UWB-MIMO antenna has exceptional multiplexing efficiency.

4.6. Group Delay

Group delay is a temporal feature of multiple-input multiple-output antennas. Figure 11 illustrates the fluctuations in the simulated group delay of the four antenna elements across the UWB spectrum. Group delay (1-1) represents the delay measured from port 1 to port 1, whereas group delays (1-2), (1-3), and (1-4) correspond to the delays from port 1 to ports 2, 3, and 4, respectively. Due to the same and symmetrical elements in the proposed MIMO antenna, group delays from ports 1 to 2 and 4 show nearly identical characteristics, as shown in Figure 11. The recommended MIMO antenna has group delays of < 1.5 ns, except at the notch frequencies. Figure 12 shows the proposed antenna measurement inside an anechoic chamber. Additionally, the efficacy of the proposed antenna was assessed by comparing it with results of previous studies, and Table 2 encapsulates the outcomes. A thorough examination of the efficacy of each antenna, as demonstrated in the table, reveals that the antenna attains a broader operational frequency spectrum and enhanced isolation while maintaining structural miniaturization.

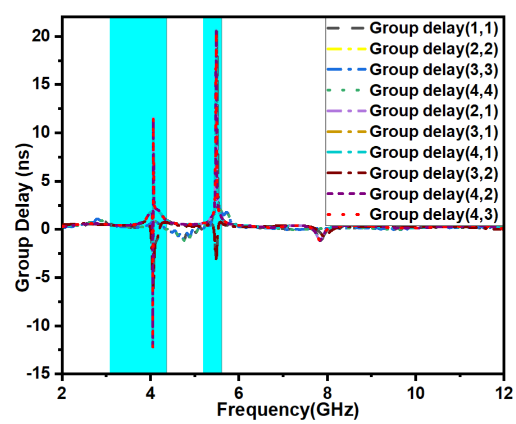

FIGURE 11. Simulated group delays.

The mutual coupling suppression (< -20 dB) in this design relies on two primary mechanisms: Orthogonal Radiator Polarization: The four microstrip-fed circular radiators are oriented perpendicular (90°) to each adjacent element. This creates orthogonal spatial polarization diversity, minimizing field coupling between adjacent ports. Defective/Modified Ground Plane Structures: Triangular ground plane cuttings and curved/stepped ground modifications near microstrip feed lines perturb cross-coupling surface currents and extend current paths, suppressing unwanted coupled surface waves between ports.

TABLE 3. Comparison with existing designs.

Ref.	Electrical Size ($\lambda_0 \times \lambda_0$)	BW (GHz)	Notched Band (GHz)	Isolation (dB)	ECC	DG (dB)	TARC (dB)	Multiplexing Efficiency	CCL (bits/s/Hz)
[27]	$0.289\lambda_0 \times 0.310\lambda_0$	3.1–10.6	-	22	< 0.02	-	-	-	-
[28]	$0.400\lambda_0 \times 0.400\lambda_0$	3.0–12.0	-	20	< 0.01	9.98	-	-	0.15
[29]	$0.310\lambda_0 \times 0.331\lambda_0$	3.1–11.0	5.5	25	< 0.02	9.95	-	-	0.20
[30]	$0.269\lambda_0 \times 0.351\lambda_0$	3.1–10.6	-	23	< 0.01	9.99	-	-	0.10
[39]	$0.46\lambda_0 \times 0.41\lambda_0$	3.1–12.5	4.6–5.9, 6.8–8.8	> 22	< 0.008	10	< -12.5	< -2	< 0.2
[40]	$0.2\lambda_0 \times 0.4\lambda_0$	3.1-12.0	5.2, 7.4	> 25	< 0.001	> 9.9	-10	0	0.2
[41]	$0.21\lambda_0 \times 0.21\lambda_0$	3.1–10.8	7.3, 8.2	> 15	< 0.05	9.5	-	-	-
[42]	$0.44\lambda_0 \times 0.48\lambda_0$	3–12	3.5–4.1, 4.43–4.79, 5.25–5.71	-2	< 0.16	-	-	-	-
[43]	$0.25\lambda_0 \times 0.39\lambda_0$	2.9–10.6	3.6–4.6, 4.9–5.5, 6.1–6.7	-20	< 0.02	> 9.99	< -10	< -1	< 0.4
Prop. Antenna	$0.377\lambda_0 \times 0.377\lambda_0$	2.9–10.6	3.1–4.3, 5.2–5.6	-20	< 0.02	9.9	< -10	< -1	< 0.2

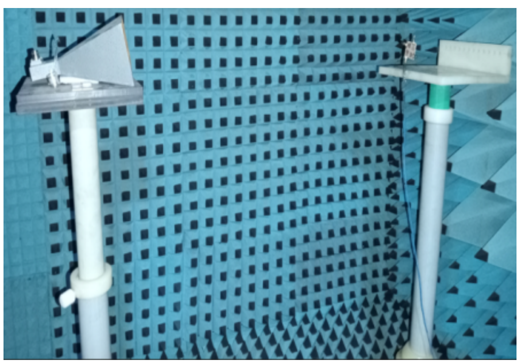

FIGURE 12. Measurement inside an anechoic chamber.

4.7. Experimental Measurement Setup

The fabricated quad-port MIMO antenna was experimentally characterized in an anechoic chamber to validate simulated radiation characteristics. The antenna under test (AUT) was positioned in the far-field region at a separation distance of (1 mm) from the transmitting reference antenna. The measurement distance was selected according to the far-field condition

$$R > \frac{2D^2}{\lambda_{\text{min}}},$$

where D is the maximum dimension of the AUT, and λ_{min} is the minimum free-space wavelength corresponding to the highest measurement frequency. The radiation characteristics were measured using a Keysight E5063A Vector Network Analyzer with the unused antenna ports terminated by 50-Ω loads. Before measurement, RF cables and the measurement path were calibrated using [SOLT], and the measured gain was corrected for the calibrated cable and system losses.

During radiation-pattern and gain measurements, the selected antenna port was excited through the calibrated measurement system, while the remaining three ports were terminated with matched 50-Ω loads. The same excitation and termination conditions were maintained for corresponding simulated and measured configurations.

4.8. Characteristic Mode Analysis

Characteristic Mode Analysis (CMA) is a systematic approach for investigating the intrinsic electromagnetic behavior of conducting structures. Rather than relying only on port excitation and S-parameters, the CMA decomposes the total surface current into a set of orthogonal characteristic modes. Each mode is uniquely defined by its eigenvalue, modal significance, characteristic angle, and current distribution. The modal significance (MS) indicates which modes actively radiate at a given frequency. The MS can be determined using Eq. (12).

$$\text{MS} = \left|\frac{1}{1 + J\lambda_i}\right| \quad (12)$$

where λ_i represents the eigenvalue of the i^{th} mode. A mode resonates when $\lambda_i = 0$ or equivalently when $\text{MS} = 1$. The characteristic angle (CA) is another metric that provides a phase-based interpretation of how stored and radiated energies of each mode are balanced. The CA is mathematically defined as

$$\alpha_i = 180^\circ - \tan^{-1}\lambda_i \quad (13)$$

Characteristic Mode Analysis (CMA) was further performed for Antenna-3, 4, 5, and 6 to validate their resonant characteristics. Figure 13 shows Modal Significance (MS) responses. Modes 2, 3, and 4 configurations were significant within 4–9 GHz, indicating their dominant role in radiation across this frequency region. Figure 14(a) shows the characteristic angle (CA) of the proposed UWB MIMO antenna. A characteristic angle close to 180° indicates resonance and efficient radiation. Modes 1–4 sequentially approach the resonance condition at different frequencies, enabling wideband operation. In contrast, Modes 5 and 6 remained away from 180°, indicating a

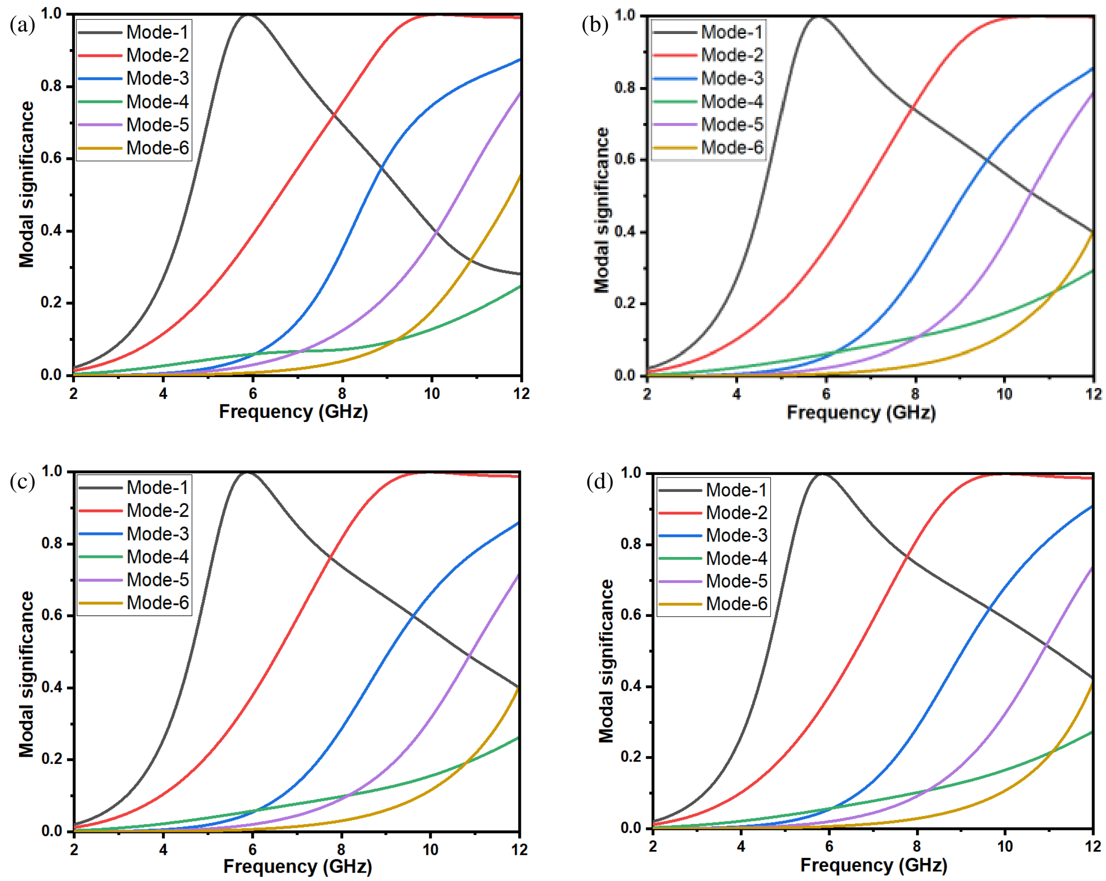

FIGURE 13. Modal significance curves obtained from Characteristic Mode Analysis for the antenna evolution process: (a) Antenna-3, (b) Antenna-4, (c) Antenna-5, and (d) Antenna-6.

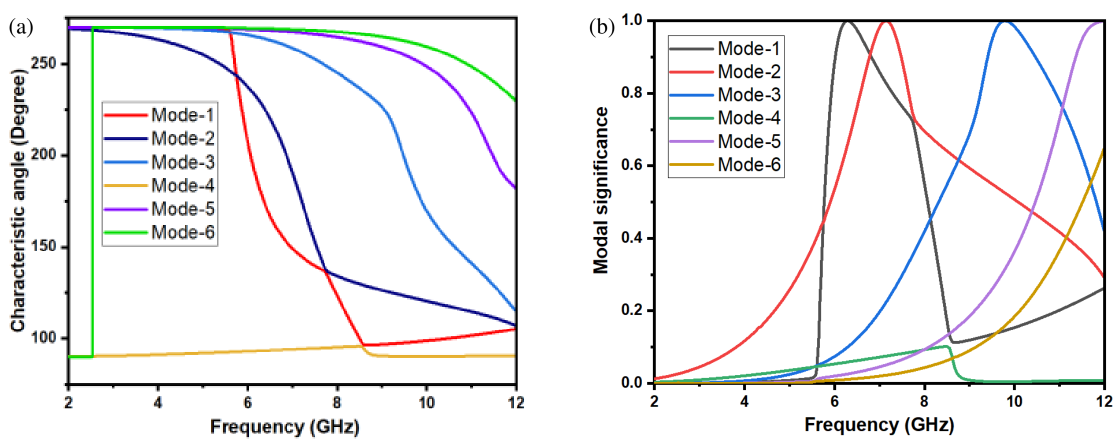

FIGURE 14. Proposed band-notched UWB MIMO antenna. (a) Characteristic angle and (b) modal significance.

negligible contribution to radiation within the operating band. Figure 14(b) shows the modal significance (MS) of the corresponding modes. A modal significance value close to 1 represents strong resonance and effective radiation. Modes 1–4 exhibit peak modal significance at different frequencies, confirming their dominant contribution across the UWB operating band. Conversely, Modes 5 and 6 maintained low modal significance over most of the frequency range, indicating weak excitation.

Combined CA and MS results show that the proposed antenna achieves wideband performance via the sequential excitation of multiple characteristic modes while suppressing non-radiating modes, ensuring stable radiation characteristics and efficient operation.

4.9. Advantages, Applications, and Limitations

The main advantages, applications, and limitations of the proposed antenna are summarized as follows.

Advantages: The proposed antenna has a compact size of $39 \times 39 \times 1.6\,\text{mm}^3$ and provides wide UWB operation from 2.9 to 10.6 GHz with dual-band rejection. It achieves high port isolation of better than 20 dB, low ECC (< 0.02), approximately 9.9 dB diversity gain, and radiation efficiency up to 90%. Band-notches are realized directly in the antenna structure using U-shaped slots, avoiding the need for additional external filtering components.

Applications: Owing to its wide bandwidth, compact size, high isolation, and good diversity performance, the proposed antenna is suitable for UWB-MIMO wireless communication applications, particularly compact wireless and portable devices. The dual-notch characteristics are also useful in applications where interference from the C-band and WLAN bands needs to be suppressed.

Limitations: The proposed antenna is fabricated on an FR-4 substrate, and its performance can be affected by fabrication tolerances, material losses, and surrounding electronic components in a practical device. In addition, the antenna performance is mainly validated through simulation and measurement of the fabricated prototype; complete integration with the remaining RF circuitry and a real wireless communication system is beyond the scope of the present work. Further optimization may therefore be required for specific practical devices and environments. Table 3 presents a comparative analysis of the proposed antenna with recently reported designs, highlighting its overall performance.

5. CONCLUSION

This study presents a miniaturized UWB-MIMO antenna with dual-band suppression characteristics, measuring $39 \times 39 \times 1.6\,\text{mm}^3$. Introducing two U-shaped slots generates notch frequency bands. Measured results indicate that the fabricated antenna demonstrates $|S_{11}| < -10\,\text{dB}$, enhanced isolation exceeding 20 dB, peak gain of 4.5 dBi, radiation efficiency fluctuating between 65% and 90%, ECC < 0.02, and TARC $< -10\,\text{dB}$ across the ultra-wideband, with the exception of two notch bands at 3.1–4.3 GHz and 5.2–5.6 GHz. All measured and simulated outcomes demonstrate that the proposed quad-port MIMO antenna is a suitable choice for UWB applications.

REFERENCES

[1] Win, M. Z. and R. A. Scholtz, "Ultra-wide bandwidth time-hopping spread-spectrum impulse radio for wireless multiple-access communications," *IEEE Transactions on Communications*, Vol. 48, No. 4, 679–689, Apr. 2000.

[2] Ghavami, M., L. Michael, and R. Kohno, *Ultra Wideband Signals and Systems in Communication Engineering*, 2nd ed., John Wiley & Sons, Chichester, U.K., 2007.

[3] Schantz, H. G., *The Art and Science of Ultra-Wideband Antennas*, Artech House, Norwood, MA, USA, 2005.

[4] Balanis, C. A., *Antenna Theory: Analysis and Design*, 4th ed., Wiley, Hoboken, NJ, USA, 2016.

[5] Taylor, J. D., *Introduction to Ultra-Wideband Radar Systems*, CRC Press, Boca Raton, FL, USA, 1994.

[6] Qu, S.-W., J.-L. Li, and Q. Xue, "A band-notched ultrawideband printed monopole antenna," *IEEE Antennas and Wireless Propagation Letters*, Vol. 5, 495–498, 2006.

[7] Zhang, Y., W. Hong, C. Yu, Z.-Q. Kuai, Y.-D. Don, and J.-Y. Zhou, "Planar ultrawideband antennas with multiple notched bands based on etched slots on the patch and/or split ring resonators on the feed line," *IEEE Transactions on Antennas and Propagation*, Vol. 56, No. 9, 3063–3068, Sep. 2008.

[8] Li, W. T., X. W. Shi, and Y. Q. Hei, "Novel planar UWB monopole antenna with triple band-notched characteristics," *IEEE Antennas and Wireless Propagation Letters*, Vol. 8, 1094–1098, 2009.

[9] Liu, X. L., Y.-Z. Yin, P. A. Liu, J. H. Wang, and B. Xu, "A CPW-fed dual band-notched UWB antenna with a pair of bended dual-L-shape parasitic branches," *Progress In Electromagnetics Research*, Vol. 136, 623–634, 2013.

[10] Zhu, F., S. Gao, A. T. S. Ho, R. A. Abd-Alhameed, C. H. See, T. W. C. Brown, J. Li, G. Wei, and J. Xu, "Multiple band-notched UWB antenna with band-rejected elements integrated in the feed line," *IEEE Transactions on Antennas and Propagation*, Vol. 61, No. 8, 3952–3960, Aug. 2013.

[11] Ojaroudi, M., G. Ghanbari, N. Ojaroudi, and C. Ghobadi, "Small square monopole antenna for UWB applications with variable frequency band-notch function," *IEEE Antennas and Wireless Propagation Letters*, Vol. 8, 1061–1064, 2009.

[12] Ojaroudi, M. and N. Ojaroudi, "Ultra-wideband small rectangular slot antenna with variable band-stop function," *IEEE Transactions on Antennas and Propagation*, Vol. 62, No. 1, 490–494, 2014.

[13] Wang, Q. and Y. Zhang, "Design of a compact UWB antenna with triple band-notched characteristics," *International Journal of Antennas and Propagation*, Vol. 2014, No. 1, 892765, 2014.

[14] Liang, J., C. C. Chiau, X. Chen, and C. G. Parini, "Study of a printed circular disc monopole antenna for UWB systems," *IEEE Transactions on Antennas and Propagation*, Vol. 53, No. 11, 3500–3504, Nov. 2005.

[15] Ma, T.-G. and S.-K. Jeng, "Planar miniature tapered-slot-fed annular slot antennas for ultrawide-band radios," *IEEE Transactions on Antennas and Propagation*, Vol. 53, No. 3, 1194–1202, Mar. 2005.

[16] Azim, R., M. T. Islam, and N. Misran, "Compact tapered-shape slot antenna for UWB applications," *IEEE Antennas and Wireless Propagation Letters*, Vol. 10, 1190–1193, 2011.

[17] Liu, Y., Z. Chen, and S. Gong, "Triple band-notched aperture UWB antenna using hollow-cross-loop resonator," *Electronics Letters*, Vol. 50, No. 10, 728–730, May 2014.

[18] Cai, L. Y., Y. Li, G. Zeng, and H. C. Yang, "Compact wideband antenna with double-fed structure having band-notched characteristics," *Electronics Letters*, Vol. 46, No. 23, 1534–1536, Nov. 2010.

[19] Liu, J., S. Gong, Y. Xu, X. Zhang, C. Feng, and N. Qi, "Compact printed ultra-wideband monopole antenna with dual band-notched characteristics," *Electronics Letters*, Vol. 44, No. 12, 710–711, 2008.

[20] Ding, J., Z. Lin, Z. Ying, and S. He, "A compact ultra-wideband slot antenna with multiple notch frequency bands," *Microwave and Optical Technology Letters*, Vol. 49, No. 12, 3056–3060, 2007.

[21] Molisch, A. F., *Wireless Communications*, 2nd ed., Wiley, Hoboken, NJ, USA, 2011.

[22] Tse, D. and P. Viswanath, *Fundamentals of Wireless Communication*, Cambridge University Press, Cambridge, U.K., 2005.

[23] Larsson, E. G., O. Edfors, F. Tufvesson, and T. L. Marzetta, "Massive MIMO for next generation wireless systems," *IEEE Communications Magazine*, Vol. 52, No. 2, 186–195, Feb. 2014.

[24] Sharawi, M. S., *Printed MIMO Antenna Engineering*, Artech House, MA, USA, 2014.

[25] Sharawi, M. S., "Current misuses and future prospects for printed multiple-input, multiple-output antenna systems [wireless corner]," *IEEE Antennas and Propagation Magazine*, Vol. 59, No. 2, 162–170, Apr. 2017.

[26] Blanch, S., J. Romeu, and I. Corbella, "Exact representation of antenna system diversity performance from input parameter description," *Electronic Letters*, Vol. 39, No. 9, 705–707, May 2003.

[27] Zhang, S. and G. F. Pedersen, "Mutual coupling reduction for UWB MIMO antennas with a wideband neutralization line," *IEEE Antennas and Wireless Propagation Letters*, Vol. 15, 166–169, 2016.

[28] Li, J.-F., Q.-X. Chu, Z.-H. Li, and X.-X. Xia, "Compact dual band-notched UWB MIMO antenna with high isolation," *IEEE Transactions on Antennas and Propagation*, Vol. 61, No. 9, 4759–4766, Sep. 2013.

[29] Iqbal, A., O. A. Saraereh, A. Bouazizi, and A. Basir, "Metamaterial-based highly isolated MIMO antenna for portable wireless applications," *Electronics*, Vol. 7, No. 10, 267, 2018.

[30] Singh, H. V. and S. Tripathi, "Compact UWB MIMO antenna with cross-shaped unconnected ground stub using characteristic mode analysis," *Microwave and Optical Technology Letters*, Vol. 61, No. 7, 1874–1881, Jul. 2019.

[31] Wong, H., K.-M. Luk, C. H. Chan, Q. Xue, K. K. So, and H. W. Lai, "Small antennas in wireless communications," *Proceedings of the IEEE*, Vol. 100, No. 7, 2109–2121, Jul. 2012.

[32] Wong, K.-L., C.-Y. Tsai, and J.-Y. Lu, "Two asymmetrically mirrored gap-coupled loop antennas as a compact building block for eight-antenna MIMO array in the future smartphone," *IEEE Transactions on Antennas and Propagation*, Vol. 65, No. 4, 1765–1778, 2017.

[33] Chen, Y. and C.-F. Wang, *Characteristic Modes: Theory and Applications in Antenna Engineering*, John Wiley & Sons, Hoboken, NJ, USA, 2015.

[34] Harrington, R. and J. Mautz, "Theory of characteristic modes for conducting bodies," *IEEE Transactions on Antennas and Propagation*, Vol. 19, No. 5, 622–628, Sep. 1971.

[35] Cabedo-Fabres, M., E. Antonino-Daviu, A. Valero-Nogueira, and M. F. Bataller, "The theory of characteristic modes revisited: A contribution to the design of antennas for modern applications," *IEEE Antennas and Propagation Magazine*, Vol. 49, No. 5, 52–68, Oct. 2007.

[36] Zhang, Q., R. Ma, W. Su, and Y. Gao, "Design of a multimode UWB antenna using characteristic mode analysis," *IEEE Transactions on Antennas and Propagation*, Vol. 66, No. 7, 3712–3717, Jul. 2018.

[37] Zhang, Q. and Y. Gao, "Compact low-profile UWB antenna with characteristic mode analysis for UHF TV white space devices," *IET Microwaves, Antennas & Propagation*, Vol. 11, No. 11, 1629–1635, Aug. 2017.

[38] Wu, W. and Y. P. Zhang, "Analysis of ultra-wideband printed planar quasi-monopole antennas using the theory of characteristic modes," *IEEE Antennas and Propagation Magazine*, Vol. 52, No. 6, 67–77, Dec. 2010.

[39] Kumar, P., T. Ali, S. Pathan, K. Nayak, T. Khan, A. A. Kishk, *et al.*, "A quad port dual band notch UWB MIMO antenna using hybrid decoupling structure," *Results in Engineering*, Vol. 23, 102551, 2024.

[40] "A compact highly isolated two- and four-port ultrawideband Multiple Input and Multiple Output antenna with wireless LAN and X-band notch characteristics based on Defected Ground Structure."

[41] Modak, S., T. Khan, T. A. Denidni, and Y. M. M. Antar, "Miniaturized self-isolated UWB MIMO planar/cuboidal antenna with dual X-band interference rejection," *AEU — International Journal of Electronics and Communications*, Vol. 143, 154020, 2022.

[42] Sushma, T., R. Gogineni, N. V. Ratnam, S. R. Babu, S. Mandava, and P. V. K. Kanth, "A miniaturized quad port highly isolated triple band notched UWB-MIMO diversity antenna," *Progress In Electromagnetics Research C*, Vol. 152, 43–53, 2025.

[43] Thotakura, H., R. Gogineni, K. S. Rao, C. K. Kumar, R. B. Sadineni, and S. Mandava, "A miniaturized highly isolated two port triple band-notched UWB MIMO antenna verified by characteristic mode analysis," *Progress In Electromagnetics Research C*, Vol. 160, 133–142, 2025.